Korean J. Chem. Eng., 34(3), 935-941 (2017)
DOI: 10.1007/s11814-016-0340-y

pISSN: 0256-1115
eISSN: 1975-7220

Effect of process parameters on the $CaCO_3$ production in the single process for carbon capture and mineralization

Arti Murnandari[*,], Jimin Kang[*,***], Min Hye Youn[*], Ki Tae Park[*], Hak Joo Kim[*], Seong-Pil Kang[*], and Soon Kwan Jeong[*,**,†]**

*Green Energy Process Laboratory, Korea Institute of Energy Research, 152 Gajeong-ro, Yuseong-gu, Daejeon 34128, Korea
**University of Science and Technology Korea, 217 Gajeong-ro, Yuseong-gu, Daejeon 34129, Korea
***Department of Chemical and Biological Engineering, Korea University, 145, Anam-ro, Sungbuk-gu, Seoul 02841, Korea
(*Received 13 July 2016 • accepted 29 November 2016*)

Abstract–The regeneration of the CO_2 capture system is the most energy-intensive process associated with CO_2 capture because high temperatures are required to desorb CO_2 from the absorbent. We propose a single process for effective CO_2 capture and mineralization as a substitute for desorption of absorbed CO_2, producing high value-added $CaCO_3$. A saturated 2-amino-2-methyl-1-propanol (AMP) solution was used as a carbonate source, and calcium chloride ($CaCl_2$) was used as a calcium ion source to precipitate $CaCO_3$. A semi-batch reactor was used to investigate the effects of the mixing rate, temperature, and amount of calcium added during the $CaCO_3$ precipitation process. During the mineralization reaction, the absorbed CO_2 in AMP solution instantly converted into white $CaCO_3$ precipitant with 97.4% conversion. The stirring rate provided a reciprocal effect on the crystal size, whereas the temperature and Ca/CO_2 molar ratio appeared to affect the crystal morphology.

Keywords: CO_2 Utilization, AMP Process, Mineralization, Calcium Carbonate, Morphology

INTRODUCTION

Amine scrubbing gas sweetening is a mature and widely used process in industrial applications. It has been used to remove acidic gas over the last 70 years in the oil and chemical industries; however, its use in carbon capture and storage (CCS) systems has generated a concern of global warming [1-3]. Thermal treatment is used in CCS processes to recycle the amine solvent. Although amine scrubbing technology is mature, its energetic requirements are estimated to contribute 70-100% of the electricity costs associated with the CCS process [4], mainly because of the energy requirements of the regeneration process. The electricity costs of conventional CCS technologies may potentially be offset by introducing novel technologies and configurations for aqueous absorption-regeneration processes, such as those proposed recently by several research groups [5-17]. The combination of solvent and process configurations has captured the focus of advanced development efforts. Solvents studies have identified a variety of amines with potential utility, for instance, promoted monoethanolamine (MEA), promoted tertiary amines, and hindered amines [5-7]. Hindered amines react rapidly with CO_2, in a high capacity, and they have low-energy requirements for regeneration [8]. These amines have been proposed as improved absorbents.

Several process configurations have been explored in combination with MEA scrubbing technologies in power plants, including ultra-supercritical pulverized coal (USC PC), natural gas combined cycle (NGCC), and integrated gasification combined cycle (IGCC) power plants [9,10]. The downside to this method is that it ultimately reduces the performance and efficiency of power generation in power plant, thus intensifying flue gas treatments like intercooling installation in absorber; the result shows energy saving 2-7% for MEA and DEA system simulation [11]. The addition of a column to increase the lean amine vapor pressure can reduce the reboiler duty by improving vapor stripping; nonetheless, additional electricity is needed to run the compressor [12,13]. Another flow sheet configuration modification is based on a split-flow configuration in which multiple feeds lead into the absorber, and the feed to the stripper is staged [14]. The stripper was modified to employ a matrix stripper that reduced the energy penalty by 22% when paired with a stripper feed flow cross-exchanging heat configuration [15]. Leites et al. and Aroonwilas described an internal exchange stripper configuration that permitted heat exchange inside the stripper, that is, the flashing speed enabled heat exchange between the rich amine solution in the middle part of the stripper and lean amine solution that was exiting the bottom of the exchanger. The performance of this configuration, however, was lower than that of the matrix stripper configuration [16,17].

A novel approach to CO_2 sequestration has involved mineralizing CO_2, instead of using a thermal regeneration configuration. The mineralization of CO_2 to form a stable carbonate mineral has received significant attention. The CO_2 mineralization reaction is a thermodynamically favorable process at moderate temperatures and pressures.

Natural carbonation is a slow process that proceeds on geologi-

†To whom correspondence should be addressed.
E-mail: jeongsk@kier.re.kr
‡This paper is reported in the 11th China-Korea Clean Energy Workshop.

cal timescales, depending on the acidity of the rainwater. Carbonation from captured CO_2 is expected to accelerate the carbonation of the earth's crust. Calcium carbonate is one of the products of mineral carbonation. The reaction is exothermic and can proceed through the Kraft pulping method, in which carbonation occurs directly in solution [18]. Steps are shown in Eqs. (1)-(4).

$$CO_{2(g)} \rightleftharpoons CO_{2(aq)} \quad (1)$$

$$CO_{2(aq)} + OH_{(aq)}^{-} \rightleftharpoons HCO_{3(aq)}^{-} \quad (2)$$

$$HCO_{3(aq)}^{-} + OH_{(aq)}^{-} \rightleftharpoons CO_{3(aq)}^{2-} + H_2O_{(l)} \quad (3)$$

$$Ca_{(aq)}^{2+} + CO_{3(aq)}^{2-} \rightleftharpoons CaCO_{3(s)} \quad (4)$$

Industrial applications of CO_2 mineralization processes require the direct or indirect mineral carbonation reactions to be accelerated. Direct carbonation routes in CCS tend to suffer from low efficiency because contact between the solid calcium source and the dissolved CO_2 is limited to the relatively small surface area of the solid calcium source. Direct carbonation processes with pretreatment suffer from a high energy penalty since material handling requires high temperatures to promote the reaction [19]. Indirect pretreatments are more attractive options because they separate the dissolution and precipitation steps, rendering this process applicable to raw waste materials [20]. The main problem associated with indirect carbonation is the high cost of the chemicals used in the process. The combination of carbonation and absorption processes in carbon capture technologies is advantageous for their ability to reduce the regeneration costs and utilize the captured CO_2; however, these combination strategies face many challenges associated with the reactor designs, process parameters, and product control requirements.

Calcium carbonate needs for industry processes lead to increased market demand year by year along with industries' growth depends on its properties [21]. Calcium carbonate exists in three crystal morphs: calcite, vaterite, and aragonite. Calcite as the most stable form of calcium carbonate crystals and is preferred in industrial applications, such as paper-making, pharmaceutical processes, and food processing [22]. Calcite has five different structural shapes: rhombohedral, rhomboscalenohedral, scalenohedral, scalenorhombohedral, and spheroidal [23]. Agglomerations of calcite have been observed, including truncated prismatic and chain-like agglomerates [24]. Calcite in a rhombohedral or scalenohedral shape is useful in the paper industry as filler because it can improve the optical properties of paper sheets [21]. A variety of factors can affect the shape and size of precipitated calcium carbonate (PCC). The morphology and particle size can depend on the surfactant, additives, the CO_2 flow rate during carbonation, the pH level, temperature, and the initial concentration of CO_2 [25].

In the present work, CO_2 mineralization reaction was carried out during the sequestration of CO_2 dissolved in an aqueous amine solution. AMP was used as the absorbent and produced carbamate and bicarbonate ions. The reaction between the CO_2 and the amine proceeded according to the following pathway:

$$RNH_2 + CO_2 \rightarrow RNHCOO^{-} + H^{+} \quad (5)$$

$$RNHCOO^{-} + H_2O \rightarrow RNH_2 + HCO_3^{-} \quad (6)$$

Vucak et al. investigated the morphologies of calcium carbonate during carbonation in the presence of MEA and nitric acid [26]. Vaterite was obtained at low temperatures, and aragonite was obtained at high temperatures, using calcium oxide as the calcium ion source. The precipitation of calcium carbonate in the presence of carbamate ions and calcium acetate has also been reported [27]. At low reactant concentrations, calcite was formed at all temperatures, but at high concentrations, a mixture of vaterite and calcite was formed.

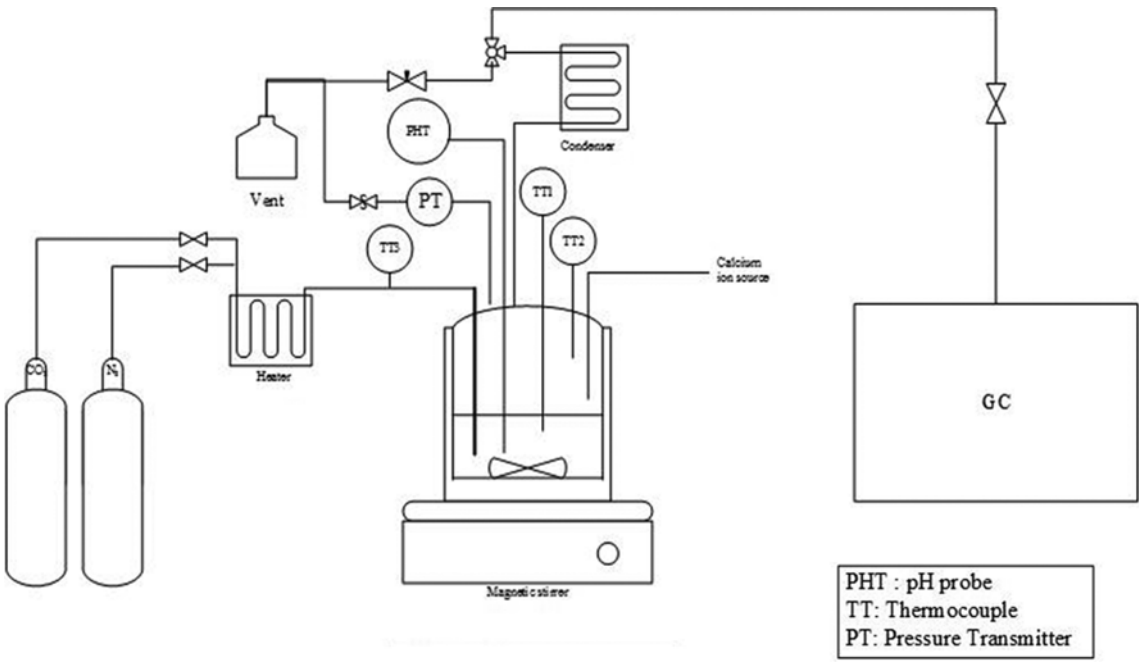

Fig. 1. Schematic diagram of experimental set-up.

Previous studies of precipitation control in a batch reactor and in the presence of an amine-saturated liquid after absorption involved a separate mineralization step [28,29]. In this work, all reactions associated with CO_2 mineralization were conducted in a semi-batch reactor under distinct reaction conditions. After the CO_2 absorption had reached a maximum amine loading level, the calcium source was injected into the system, and the final product was harvested at the end of the reaction. The effects of the process parameters, including the temperature, mixing rate, reaction time, and calcium source, on the shape and crystal structure of the resulting $CaCO_3$ were investigated to identify the optimal conditions for CO_2 mineralization in a semi-batch system.

EXPERIMENTAL

1. Single Step Absorption-mineralization Procedure

Fig. 1 shows the experimental setup used to mineralize a CO_2-saturated amine solution. A glass reactor with a stainless steel cover and a water circulating bath was used in the experiment. The saturated CO_2 solution was prepared through amine absorption. A preheated gas mixture comprising 30% CO_2 and 70% N_2 was introduced into the 10 wt% 2-amino-2-methyl-1-propanol (90%, technical grade, Sigma Aldrich) solution until the gas chromatograph indicated a constant CO_2 content in the output gas stream. Anhydrous granular calcium chloride (93% purity, Sigma Aldrich) was used as a source of calcium ions in the aqueous solution and was injected into the vessel using a syringe. The effects of the mineralization conditions on the $CaCO_3$ production were investigated by preparing a series of precipitated calcium carbonate (PCC) samples at different stirring speed (X), temperatures (T), and injected calcium ratios (C) per 1 mole CO_2. The prepared PCC samples were denoted PCC_RPM_X (X=100, 400, and 600), PCC_TEMP_T (T=20, 40, 60, and 80), and PCC_$CaCl_2$_C (C=0.5, 1, and 2), respectively. The precipitated calcium carbonate was harvested from the reactor and separated from the liquid by decantation, followed by drying in an oven incubator at 80 °C for 24 hours.

2. Characterization of the Produced $CaCO_3$

The powdered calcium carbonate produced was measured using an X-ray diffractometer, Rigaku DMAX-2500, and a cold field emission scanning electron micrograph (SEM). The gas chromatograph used a carboxen packed column and a TCD detector to analyze the output gas. The moles of CO_2 loaded in the amine solution was calculated as follows:

$$\mathrm{Moles(N)}_{CO_2} = \frac{V_g \cdot P}{RT} \tag{7}$$

$$\mathrm{N}(l)_{CO_2} = \mathrm{Ninput(g)}_{CO_2} - \mathrm{Noutput(g)}_{CO_2} \tag{8}$$

The amine loading (α) and moles of amine were calculated as:

$$\alpha = \frac{\mathrm{N}(l)_{CO_2}}{\mathrm{N}_{amine}} \tag{9}$$

$$\mathrm{N}_{amine} = \frac{\mathrm{Mass}_{amine}}{\mathrm{Mass\ molecular}_{amine}} \tag{10}$$

The total loading of CO_2 in the amine (α) was calculated by integrating the moles CO_2 absorbed by the amine over time.

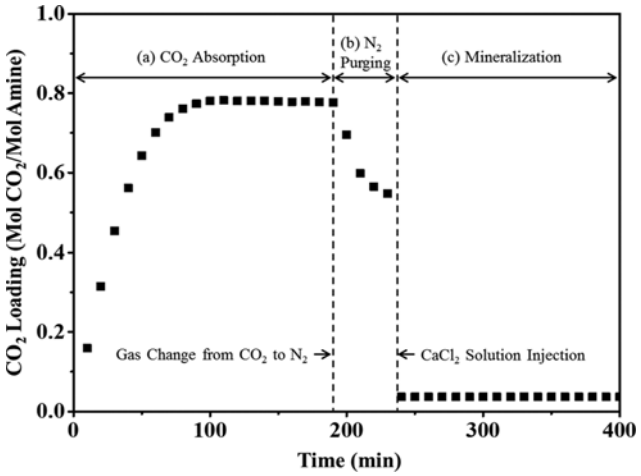

Fig. 2. CO_2 Loading curve with different process condition: CO_2 Absorption (a), N_2 purging (b), Mineralization via a reaction with calcium ions (c).

RESULTS AND DISCUSSION

1. Single Process for CO_2 Absorption-mineralization

The effects of the process condition on the CO_2 loading in the single process of CO_2 absorption-mineralization were investigated. In general, CO_2 can be regenerated physically or chemically. Physically absorbed CO_2 onto an amine sorbent could be desorbed by nitrogen purging. Different from physically absorbed CO_2, chemically absorbed CO_2 molecules require significant amounts of heat to achieve desorption from the amine sorbent. Furthermore, it is necessary for a follow-up process because the captured CO_2 has to be stored or converted to other stable forms of CO_2. Mineralization is one method of sequestering and storing CO_2 captured in a stable carbonate, thereby precluding the need for energy to compress the CO_2 in gas phase storage.

Fig. 2 plots the CO_2 absorption-desorption curves of a 10 wt% aqueous AMP solution prepared using different process conditions: CO_2 Absorption (a), N_2 purging (b), Mineralization via a reaction with calcium ions (c). In our semi-batch system, the 10 wt% aqueous AMP solution absorbed around 0.75 mol CO_2/mol amine at 40 °C and 1.2 bar. After the absorption process reached an equilibrium state (Fig. 2(a)), the gas flow changed from CO_2 to nitrogen at the same temperature and flow rate because the physically absorbed CO_2 could be desorbed from the amine absorbent during the N_2 purging process, as shown in Fig. 2(b). Then mineralization was conducted by injection of calcium chloride solution with the same molar ratio of the absorbed CO_2. Most absorbed CO_2 immediately reacted with the calcium ions to produce a white $CaCO_3$ precipitant. After mineralization, the residual CO_2 concentration was measured to be only 0.019 moles CO_2 in 1 mole AMP solution, and the efficiency of CO_2 conversion into a mineral carbonate was 97.4%. These results revealed that mineralization could be an effective regeneration method for CO_2 desorption from an AMP system.

2. Effect of the Mixing Rate on the Crystallization of the Precipitated Calcium Carbonate

The effects of the mixing conditions on the crystallization of

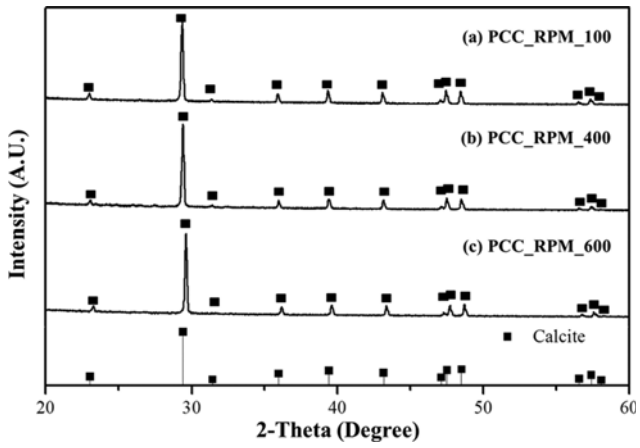

Fig. 3. X-ray diffractogram of PCC_RPM_X (X=100, 400, and 600) prepared with different stirring rates (X) of 100, 400, and 600 rpm.

calcium carbonate were investigated by conducting CO_2 mineralization at different stirring speeds. Fig. 3 presents the X-ray diffractogram of PCC_RPM_X (X=100, 400, and 600) prepared with different stirring rates (X) of 100, 400, and 600 rpm, respectively. All samples obtained yielded XRD peaks associated with calcite $CaCO_3$, the most stable polymorph of calcium carbonate. The average crystallite size in PCC_RPM_X (X=100, 400, and 600) was estimated from the centroid peak positions using the Jade plus program to minimize deviations of the peak reflection from their predicted positions. The calculated calcium carbonate crystal size increased in the order of PCC_RPM_100 (19 nm), PCC_RPM_400 (24 nm), and PCC_RPM_600 (29 nm). SEM images of the precipitated $CaCO_3$ crystals agreed with the XRD results, as shown in Fig. 4.

The PCC_RPM_600 sample prepared at a higher stirring rate promoted the growth of larger crystals surface, instead of producing new crystals. As the surface reaction proceeded, the mass transfer was controlled by convection (liquid transfer) and diffusion. At this stage, transport of the Ca^{2+} ion solute was greater when adsorbed onto the crystal surface, so the reaction on the surface of the crystal proceeded preferentially over the formation of new crystals. In this case, Ostwald ripening occurred rapidly, as indicated by the intermittent cascade in solution, which made it difficult to observe [30]. Agglomeration occurred as crystals collided and adhered to generate larger particles. Small nuclei subsequently dissolved, and larger crystals were formed [31]. Reciprocally, a lower stirring rate generated smaller crystals.

Calcium carbonate crystals prepared at various stirring speeds from calcium chloride formed calcite precipitates. As mentioned earlier, calcite can assume any of five structural shapes [24,25,32]. Fig. 5 presents diagrams of the calcite structural shapes. Although the stirring speed did not affect the morphology of the calcite, the cubic shape of the calcite was distorted into a diamond shape to form scalenohedral calcite. Fig. 4 shows that the PCC_RPM_400 sample formed a rhombohedral shape. As the stirring speed increased to 600 RPM, the PCC shape produced shifted from rhombohedral to scalenohedral, as shown in the SEM image. The scalenohedral shift arose from alpha crystal formation in the presence of additives, such as amino groups [33]. Lopez-Periago et al. reported that a high yield could be achieved by applying ultrasonic agitation to the system [34].

3. Effects of the Temperature on the Crystallization of the Precipitated Calcium Carbonate

A series of PCC_TEMP_T (T=20, 40, 60, and 80) samples was prepared by CO_2 mineralization at different absorption and precipitation temperatures over the range 20-80 °C. As the AMP solution absorbed the carbon dioxide, the total loading of CO_2 in the amine (α) was inversely proportional to the temperature. These

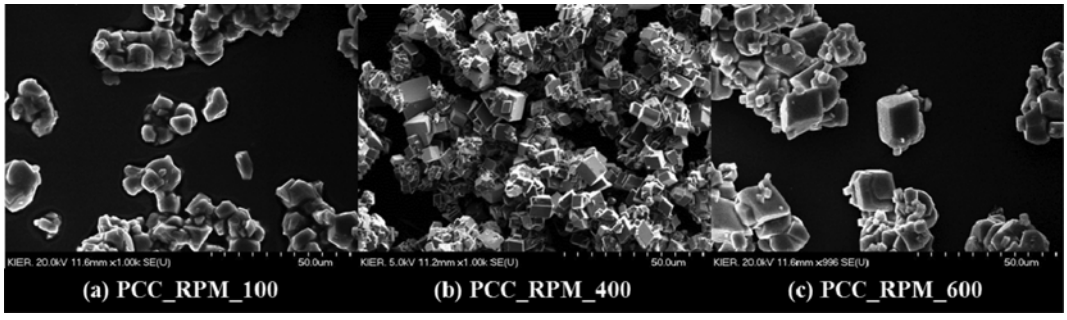

Fig. 4. SEM image of PCC_RPM_X (X=100, 400, and 600) prepared with different stirring rates (X) of 100, 400, and 600 rpm.

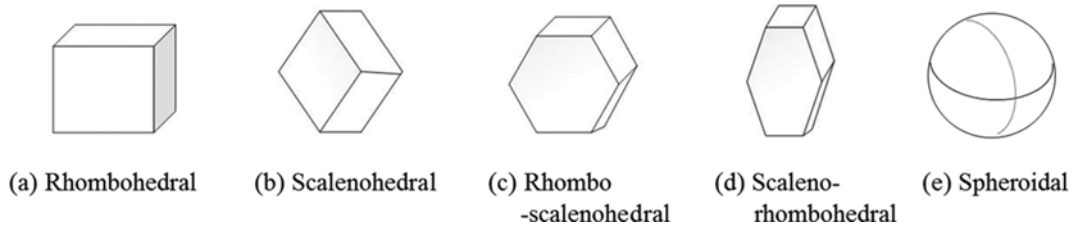

Fig. 5. Diagrams of the calcite structural shapes.

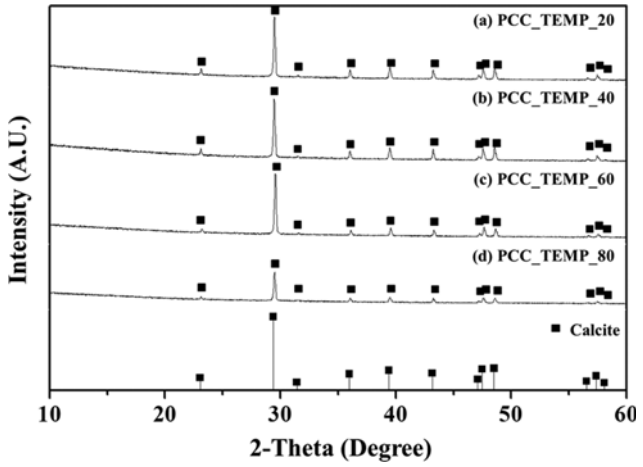

Fig. 6. X-Ray diffractograms of PCC_TEMP_T (T=20, 40, 60, and 80) formed with different temperature (T) of 20 °C (a), 40 °C (b), 60 °C (c), and 80 °C (d).

Table 1. Summary of the CO_2 loading levels in the amine solution after absorption, and the calculated $CaCO_3$ crystal sizes after mineralization at different temperatures

	Temperature of absorption and mineralization (°C)			
	20	40	60	80
CO_2 loading (mol-CO_2/mol amine)	0.843	0.749	0.558	0.398
Crystal size (nm)	23	24	18	15

results agreed with those obtained by Kim et al. (2012) and Shariff et al. (2011) using AMP [35,36]. Fig. 6 shows the X-ray diffraction patterns obtained from the PCC_TEMP_T (T=20, 40, 60, and 80) samples dried at 80 °C. Despite differences in the CO_2 loading, all PCC_TEMP_T (T=20, 40, 60, and 80) samples showed the characteristic XRD peaks indicating the formation of calcite $CaCO_3$, as shown in Fig. 6. On the other hand, the crystal size calculated from the XRD peaks was affected by the temperature, as listed in Table 1. Table 1 summarizes the CO_2 loading levels in the amine solution after absorption and the calculated $CaCO_3$ crystal sizes after mineralization at different temperatures. The trend in the crystal sizes of PCC_TEMP_T (T=20, 40, 60, and 80) was obtained from the XRD pattern. The crystallite size tended to decrease as the temperature increased or as the concentration of dissolved CO_2 decreased [37]. In this experiment, however, the crystal size did not follow a clear trend. Instead, the morphology shape changed with the temperature, even though the CO_2 concentration in the liquid decreased with increasing temperature.

Fig. 7 shows SEM images of the PCC_TEMP_T (T=20, 40, 60, and 80) samples. The $CaCO_3$ samples exhibited different agglomeration structures at each temperature, despite the fact that all samples assumed the same calcite crystal structures. The steric hindrance of the primary amine in AMP resulted in a pKa that exceeded the pKa values of other primary amines. At higher temperatures, the pH of absorption exceeded the pH of the initial conditions for

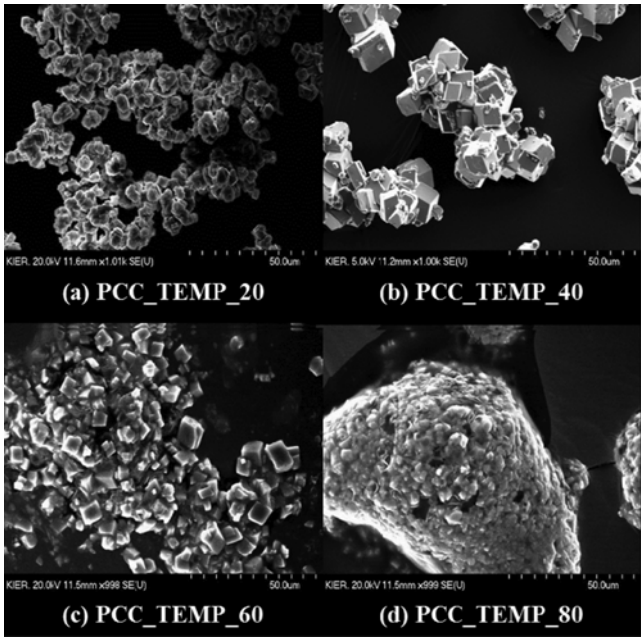

Fig. 7. SEM images of PCC_TEMP_T (T=20, 40, 60, and 80) formed with different temperature (T) of 20 °C (a), 40 °C (b), 60 °C (c), and 80 °C (d).

precipitation due to subjacent loading of CO_2. The CO_2 loading in the amine (α) and the pH of the supersaturated solution contributed to the crystal formation process. Gomez-Morales et al. investigated the effects of the initial pH on the morphology of a crystal carbonate. As the solution pH increased, vaterite shape induced more than calcite. Tai et al. explained that the initial supersaturation conditions affected the critical crystal size at a certain supersaturation value; therefore, more $CaCO_3$ crystal nuclei were generated under higher supersaturated conditions [38].

In the PCC_TEMP_20 sample, rhombohedral calcite agglomerates were formed. Kawano et al. (2002) indicated that the coexistence of calcium chloride and sodium carbonate under high supersaturation conditions promoted the formation of flat surface bounded rhombohedral calcite [39]. As the temperature increased, the calcite shape was overwhelmed by irregular crystals across its surface, thereby forming a spheroidal calcite structure (Fig. 7(c) and 7(d)). In this state, aggregation of the precipitated calcium carbonate (PCC) led to the gelation of the reaction mixture. This gel was held together by van der Waals interactions and easily collapsed [40]. The PCC_TEMP_80 sample in sticky mixture form as the final product was harvested at 80 °C, making it difficult to dry. Keith and Padden in 1963 found that the spherulitic growth of calcite usually occurred in a viscous magma, and polymers crystallized from the melt in the presence of certain thickeners [41]. The present study suggested that the high temperature of the precipitation reaction formed calcite crystals of $CaCO_3$, but the agglomeration structure shifted to a spheroidal structure. Calcite agglomeration depended strongly on the temperature.

4. Effects of the Calcium Concentration on the Crystallization of the Precipitated Calcium Carbonate

The calcium feed ratio relation to the CO_2 absorbed in the amine

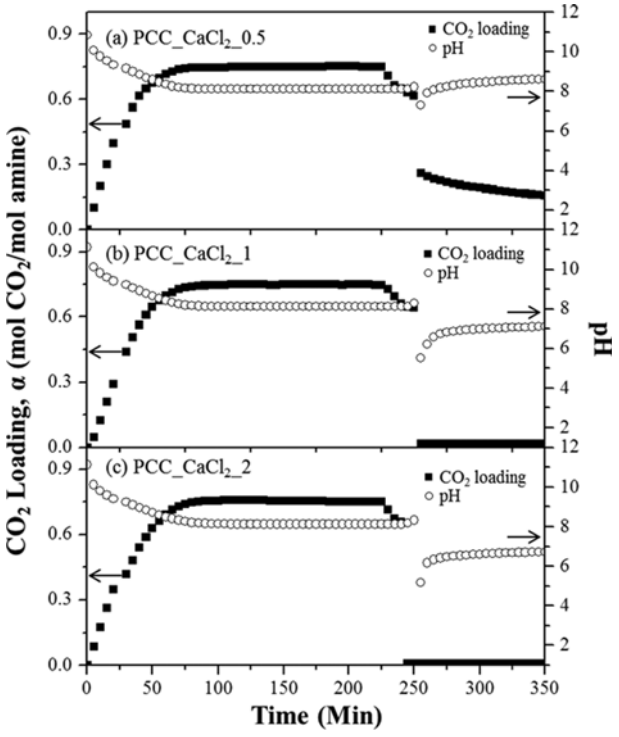

Fig. 8. Time profile of PCC_$CaCl_2$_C (C=0.5, 1, and 2) with different Ca^{2+}/CO_2 ratio (C) of 0.5 (a), 1 (b), and 2 (c).

affected the crystal formation process. These effects were investigated by conducting CO_2 mineralization over a Ca^{2+}/CO_2 ratio range of 0.5-2. Fig. 8 shows the time profiles of mineralization at each calcium concentration (C), indicated by PCC_$CaCl_2$_C (C=0.5, 1, and 2). Given fixed initial pH and absorption conditions, the final pH and CO_2 loading levels varied significantly with the calcium feed concentration.

The PCC_$CaCl_2$_0.5 sample, which was deficient of a calcium ion source, displayed a decrease in the pH to 7.3 after injection of $CaCl_2$; however, this pH recovered to its initial state. The change in the CO_2 loading level in the PCC_$CaCl_2$_0.5 sample indicated that the added calcium ions were not sufficient to react with the absorbed CO_2. As the Ca^{2+}/CO_2 molar ratio increased, however, the pH change increased, as compared with the PCC_$CaCl_2$_0.5 sample. The added calcium chloride was consumed to simultaneously form calcium carbonate and a chloric acid. After injection, a significant decrease in the pH indicated that chloric acid was formed by the reaction between the chloride ions and water. The injection of $CaCl_2$ resulted in a decrease in the pH to 5 and increased again to around 7 for both the PCC_$CaCl_2$_1 and PCC_$CaCl_2$_2 samples. These results suggested that the chloride ions coexisted in solution as chlorine ions and bicarbonate ions, causing a decrease in pH to 5. The presence of chlorine ions attracted protons from the bicarbonate ions in the saturated liquid, thereby releasing the carbonate ions to bond with calcium. The formation of calcium carbonate increased the pH until all calcium and carbonate ions in the solution had reacted.

Fig. 9 shows SEM images of the PCC_$CaCl_2$_C (C=0.5, 1, and 2) samples. As shown in Fig. 9(a), the PCC_$CaCl_2$_0.5 sample comprised a mixture of calcite and vaterite crystals under calcium-deficient conditions. The addition of calcium ions in a stoichiometric ratio (PCC_$CaCl_2$_1) resulted in the formation of rhombohedral calcite. Low concentration of Ca^{2+} induced high supersaturation condition; thus, vaterite crystal was formed [42]. Ammonium ions (NH_4^+) have been reported to promote the formation of rhombohedral crystals because ammonium has a large ionic radius that is hard to fit on spindle-like calcium carbonate crystals, exerting rhombohedral shape [43]. Another shift in the calcite agglomeration behavior was observed in the PCC_$CaCl_2$_2 sample in the presence of excess calcium ions. Abundant calcium ions in solution induced the formation of vaterite, and the presence of ammonia inhibited vaterite, promoting a transformation into calcite [44]. Irregular shapes on the surfaces of the crystal indicated the formation of unstable PCCs. In the presence of excess calcium, metastable form will be induced in the system and forming on the surface of previous crystal. In this case, smaller crystals in the system consumed less matter during crystal growth than the larger crystals [45], thereby generating irregular crystals over the surfaces of the calcite agglomerates. In contrast to the results obtained by Jung et al. [43], excess calcium ions in the system induce the formation of irregular surfaces on the calcite crystals. This irregular surface is a layer of $CaCO_3$ plates as result of twinning phenomenon, which is also mentioned by Onimisi et al., in mist spray technique for PCC production [46]. The formation of irregularly shaped calcite in the presence of excess calcium ions suggests that an excess of calcium ions in the calcium carbonate precipitation reaction in the presence of AMP was undesirable.

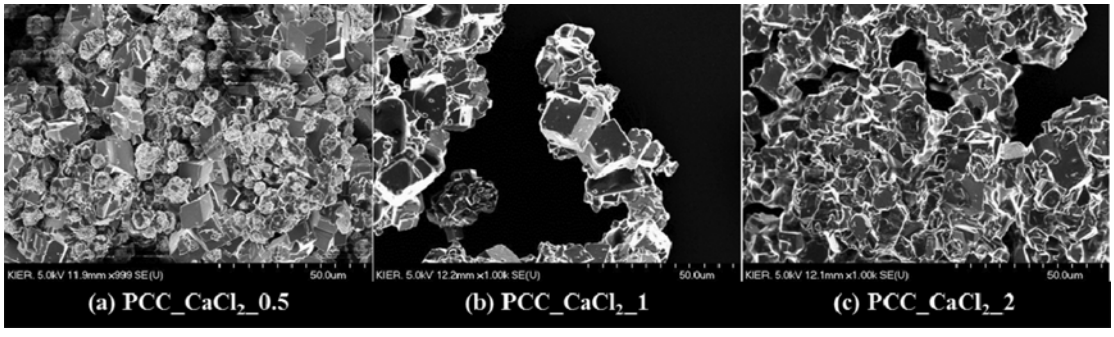

Fig. 9. SEM images of PCC_ $CaCl_2$_C (C=0.5, 1, and 2) formed with different Ca^{2+}/CO_2 ratio (C) of 0.5 (a), 1 (b), and 2 (c).

CONCLUSIONS

A single process for effective CO_2 capture and utilization was proposed. Sequestrated CO_2 in aqueous amine system was mineralized as a substitute for desorption of absorbed CO_2, producing high value-added $CaCO_3$. Mineralization combined with an absorption process could be an effective method in terms of CO_2 sequestration, CO_2 utilization, and energy efficiency. This is because the regeneration process of amine solvent with high energy consumption problem in post-combustion process can be replaced by mineralization with mild condition. The efficiency of CO_2 conversion into a mineral carbonate was 97.4% and the amine loading after mineralization was only 0.019 mol CO_2/mol amine. The mineralization process was controlled by varying the stirring speed, temperature, and calcium concentration to study the effects of the process variables on the PCC crystal formation. The stirring rate inversely affected the calcium carbonate crystal size, and the temperature affected the morphology of the formed crystal. Rhombohedral calcite was obtained at 400 RPM, 40 °C, and at a Ca^{2+}/CO_2 mole ratio of 1 in a semi-batch system.

ACKNOWLEDGEMENT

This work was conducted under the framework of the Research and Development Program of the Korea Institute of Energy Research (KIER, B7-2431-01).

REFERENCES

1. M. Lucquiaud and J. Gibbins, *Chem. Eng. Res. Des.*, **89**, 1553 (2011).
2. M. Wang, A. Lawal, P. Stephenson, J. Sidders and C. Ramshaw, *Chem. Eng. Res. Des.*, **89**, 1609 (2011).
3. J. Lim, D. H. Kim, Y. Yoon, S. K. Jeong, K. T. Park and S. C. Nam, *Energy Fuels*, **26**, 3910 (2012).
4. S. S. Warudkar, K. R. Cox, M. S Wong and G. J. Hirasaki, *Int. J. Greenh. Gas. Con.*, **16**, 342 (2013).
5. H. Dang and G. T. Rochelle, *Sep. Sci. Technol.*, **38**, 337 (2003).
6. S. Bishnoi and G. T. Rochelle, *AIChE J.*, **48**, 2788 (2002).
7. S. Bishnoi and G. T. Rochelle, *Ind. Eng. Chem. Res.*, **41**, 604 (2002).
8. G. Sartori, W. S. Ho, D. W. Savage, G. R. Chludzinski and S. Wiechert, *Sep. Purif. Methods*, **16**, 171 (1986).
9. J. M. Beér, *Prog. Energy Combust. Sci.*, **26**, 301 (2000).
10. J. M. Beér, *Prog. Energy Combust. Sci.*, **33**, 107 (2007).
11. M. Karimi, M. Hillestad and H. F. Svendsen, *Energy Procedia*, **4**, 1601 (2011).
12. D. H. Van Wagener and G. T. Rochelle, *Chem. Eng. Res. Des.*, **89**, 1639 (2011).
13. Y. Le Moullec and M. Kanniche, *Int. J. Greenh. Gas Con.*, **5**, 727 (2011).
14. T. Neveux, Y. Le Moullec, J. P. Corriou and E. Favre, *E. Chem. Eng. Trans.*, **35**, 337 (2013).
15. B. A. Oyenekan and G. T. Rochelle, *AIChE J.*, **53**, 3144 (2007).
16. I. L. Leites, D. A. Sama and N. Lior, *Energy*, **28**, 55 (2003).
17. R. Idem, M. Wilson, P. Tontiwachwuthikul, A. Chakma, A. Veawab, A. Aroonwilas and D Gelowitz, *Ind. Eng. Chem. Res.*, **45**, 2414 (2006).
18. C. Domingo, E. Loste, J. Gómez-Morales, J. García-Carmona and J. Fraile, *J. Supercrit. Fluid*, **36**, 202 (2006).
19. A. Sanna, M. Dri, M. R. Hall and M. Maroto-valer, *Appl. Energy*, **99**, 545 (2012).
20. B. M. Bhanage and M. Arai, *Transformation and Utilization of Carbon Dioxide*, Springer Berlin Heidelberg, Berlin (2014).
21. M. Popescu, R. Isopescu, C. Matei, G. Fagarasan and V. Plesu, *Adv. Powder Technol.*, **25**, 500 (2014).
22. T. Thriveni, N. Um, S.-Y. Nam, Y. J Ahn, C. Han and J. W. Ahn, *Korean Chem. Soc.*, **51**, 107 (2014).
23. J. G. Carmona, G. Morales and R. J. Rodríguez, *Colloid Interface Sci.*, **261**, 434 (2003).
24. M. Ukrainczyk, J. Kontrec, V. Babić-Ivančić, L. Brečević and D. Kralj, *Powder Technol.*, **171**, 192 (2007).
25. B. Feng, A. K. Yong and H. An, *Mater. Sci. Eng.*, **445**, 170 (2007).
26. M. Vucak, J. Peric, M. N. Pons and S. Chanel, *Powder Technol.*, **101**, 1 (1999).
27. G. Draz, J. Prah and J. Mac, *J. Cryst. Growth*, **324**, 229 (2011).
28. M. Vinoba, M. Bhagiyalakshmi, A. N. Grace, D. H. Chu, S. C. Nam, Y. Yoon, S. H. Yoon and S. K. Jeong, *Langmuir*, **29**, 15655 (2013).
29. M. Vinoba, M. Bhagiyalakshmi, S. Y. Choi, K. T. Park, H. J. Kim and S. K. Jeong, *J. Phys. Chem.*, **118**, 17556 (2014).
30. B. B. Schroeder, D. D. Harris, S. T. Smith and D. O. Lignell, *Cryst. Growth Des.*, **14**, 1756 (2014).
31. M. Torbacke and Å. C. Rasmuson, *AIChE J.*, **50**, 3107 (2004).
32. R. Beck and J.-P. Andreassen, *AIChE J.*, **58**, 107 (2012).
33. M. Kitamura, *Cryst. Eng. Comm.*, **11**, 949 (2009).
34. A. M. López-periago, R. Pacciani, C. García-gonzález, L. F. Vega and C. Domingo, *J. Supercrit. Fluid*, **52**, 298 (2010).
35. Y. E. Kim, J. A. Lim, S. K. Jeong, Y. I. Yoon, S. T. Bae and S. C. Nam, *Bull. Korean Chem. Soc.*, **34**, 783 (2013).
36. A. M. Shariff, G. Murshid, K. K. Lau, M. A. Bustam and F. Ahmad, *World Acad Sci. Eng. Technol.*, **60**, 1050 (2011).
37. M. Kitamura, *J. Cryst. Growth*, **239**, 2205 (2002).
38. C. Y. Tai, P. Chen and S. Shih, *AIChE J.*, **39**, 1472 (1993).
39. J. Kawano, N. Shimobayashi, M. Kitamura and K. Shinoda, *J. Cryst. Growth*, **239**, 419 (2002).
40. J. Schlomach, K. Quarch and M. Kind, *Chem. Eng. Technol.*, **29**, 215 (2006).
41. H. D. Keith and F. J. Padden Jr., *J. Appl. Phys.*, **34**, 2409 (1963).
42. J. W. Ahn, J. H. Kim, H. S. Park, J. A. Kim, C. Han and H. Kim, *Korean J. Chem. Eng.*, **22**, 852 (2005).
43. T. Jung, W. Kim and C. K. Choi, *Cryst. Res. Technol.*, **40**, 586 (2005).
44. Y. S. Han, G. Hadiko, M. Fuji and M. Takahashi, *J. Cryst. Growth*, **276**, 541 (2005).
45. O. Söhnel and J. W. Mullin, *J. Cryst. Growth*, **60**, 239 (1982).
46. J. A. Onimisi, R. Ismail, K. S. Ariffin, N. Baharun and H. Bin Hussin, *Korean J. Chem. Eng.*, **33**, 2756 (2016).